

CO₂ adsorption on crystalline graphitic nanostructures

Mirian E. Casco¹, Aarón Morelos-Gómez², Sofia Magdalena Vega-Díaz³, Rodolfo Cruz-Silva³, Ferdinando Tristán-López³, Hiroyuki Muramatsu⁴, Takuya Hayashi⁵, M. Martínez-Escandell¹, Mauricio Terrones^{3,6}, Morinobu Endo^{2,3}, Francisco Rodríguez-Reinoso¹, Joaquín Silvestre-Albero^{1,*}

¹Laboratorio de Materiales Avanzados, Departamento de Química Inorgánica-Instituto Universitario de Materiales, Ctra. San Vicente-Alicante s/n, E-03080 Alicante, Spain

²Institute of Carbon Science and Technology, Shinshu University, 4-17-1 Wakasato, Nagano 380-853, Japan

³Research Center for Exotic Nanocarbons (JST), Shinshu University, Wakasato 4-17-1, Nagano 380-8553, Japan

⁴Nagaoka University of Technology, 1603-1 Kamitomioka, Nagaoka, Niigata 940-2188 Japan

⁵Faculty of Engineering, Shinshu University, 4-17-1 Wakasato, Nagano 380-853, Japan

⁶Department of Physics, Department of Chemistry, Department of Materials Science and Engineering, Center for 2-Dimensional and Layered Materials, and Materials Research Institute. The Pennsylvania State University, 104 Davey Lab., University Park, Pennsylvania 16802, USA

Nomenclature

MWCNT: multiwalled carbon nanotube

MWCNT-CN_x: nitrogen doped multiwalled carbon nanotube

MWCNT-CN_x-A: acid treated nitrogen doped multiwalled carbon nanotube

MWCNT-CN_x-NR: nitrogen doped nanoribbon

MWCNT-CO_x: non-doped multiwalled carbon nanotube

MWCNT-CO_x-A: acid treated non-doped multiwalled carbon nanotube

MWCNT-CO_x-NR: non-doped multiwalled carbon nanoribbon

Abstract

CO₂ adsorption has been measured in different types of graphitic nanostructures (MWCNTs, acid treated MWCNTs, graphene nanoribbons and pure graphene) in order to evaluate the effect of the different defective regions/conformations in the adsorption process, i.e., sp³ hybridized carbon, curved regions, edge defects, etc. This analysis has been performed both in pure carbon and nitrogen-doped nanostructures in order to monitor the effect of surface functional groups on surface created after using different treatments (i.e., acid treatment and thermal expansion of the MWCNTs), and study their adsorption properties. Interestingly, the presence of exposed defective regions in the acid treated nanostructures (e.g., uncapped nanotubes) gives rise to an improvement in the amount of CO₂ adsorbed; the adsorption process being completely reversible. For N-doped nanostructures, the adsorption capacity is further enhanced when compared to the pure carbon nanotubes after the tubes were unzipped. The larger proportion of defect sites and curved regions together with the presence of stronger adsorbent-adsorbate

interactions, through the nitrogen surface groups, explains their larger adsorption capacity observed in these studies.

Corresponding author:

Dr. Joaquín Silvestre Albero; email: joaquin.silvestre@ua.es

Tel.: +34 965909350

Fax: +34965903454

Introduction

CO₂ capture using porous solids might become an advanced technology able to mitigate the large emissions of this greenhouse gas to the atmosphere [1]. Among the different porous materials studied until now, activated carbons exhibit certain advantages such as a high adsorption capacity, both at atmospheric and high pressure, an easy regeneration and, if properly designed, a high selectivity for CO₂ towards other molecules of similar dimensions such as CH₄ and/or N₂ [2-6]. Although the large adsorption capacity on carbon materials under atmospheric pressure conditions has been preferentially associated to the presence of a highly developed specific porous structure (pores < 1.0 nm), the role of surface defect sites on the adsorption process is still not completely understood [3,4,7]. Taking into account that the structure of activated carbons is associated with a disordered arrangement of defective graphitic layers in the form of twisted lamellae, the knowledge of the adsorption process on the different surface sites and/or regions seems mandatory to better understand their excellent adsorption behavior. Another critical parameter in the design of a porous carbon for CO₂ capture concerns the control of the surface chemical functionalities. For instance, previous studies have shown that the incorporation of nitrogen functionalities within the porous structure of the carbon material give rise to an improvement in the amount of CO₂ adsorbed [8-11]. These nitrogen functionalities can be present either on the surface in the form of amines, imines, and so other functional groups, or embedded in the carbon framework after appropriate selection of a nitrogen rich carbon precursor. CO₂ adsorption improvement in these materials has been associated with the presence of stronger electrostatic interactions established between the basic nitrogen functionalities and the acidic CO₂ molecule due to the distortion of the electronic structure of the basal planes.

Theoretical calculations on graphitic surfaces have predicted a low binding energy for CO₂ physisorption (~151 meV) in non-defective graphene surfaces [12]. Using density functional theory (DFT) calculations, physisorption of the CO₂ molecule occurs in a parallel fashion on the graphene rings, the adsorption geometry being slightly distorted in the presence of oxygen surface groups [13, 14]. In addition, Bader charge analysis predicts an important distortion of the electronic structure of the basal planes in the presence of surface functionalities (oxygen atoms are highly electronegative, acting as basic adsorption sites), thus increasing the adsorption energy for CO₂ molecules, i.e., the carbon atom on the CO₂ molecule would be more attracted to the embedded oxygen functional groups [14]. A similar enhancement in the adsorption energy for CO₂ has been also predicted for defective graphene sheets, the adsorption of the CO₂ molecule taking place on top of vacancy defects, with the molecule linear axis parallel to the surface [15]. Concerning carbon nanotubes (CNTs), theoretical and experimental analysis have shown a preferential adsorption of CO₂ on the grooves and interstitial sites on bundle of single-walled nanotubes (SWCNTs); the adsorption energy being very low on the surface positions [12, 16]. Jiang and Sandler used a C₁₆₈ schwarzite to evaluate the preferential adsorption of CO₂ from other molecules, such as N₂, on different carbon configurations [17]. According to their analysis, the curved surface of the C₁₆₈ schwarzite results in an enhancement in the CO₂-carbon interaction potential compared to planar graphite. The enhancement observed can be attributed to the presence of combined sp³ and sp² hybridized carbon atoms in the curved regions when compared to planar graphite containing preferentially sp² hybridized carbon.

In summary, theoretical calculations together with experimental analyses predict important changes in the electronic density of the graphitic basal planes, and indirectly, in the adsorption potential for CO₂ depending on the nature of the carbon regions and surface defects (e.g. sp²/sp³

ratio, defective sites, surface groups, curved regions, etc.). With this in mind and in order to provide a deeper insight into the understanding of the adsorption process on carbon materials, the aim of the present paper is to evaluate the role of different surface heterogeneities (unsaturated sp^3 hybridized carbon atoms, curved regions, uncapped regions, nitrogenated sites, etc.) in the adsorption/desorption process on carbon nanostructures that could eventually be used for CO_2 capture. Selected carbon nanostructures comprise multi-walled carbon nanotubes (MWCNTs), acid treated MWCNTs and graphene nanoribbons, either pure or nitrogen-functionalized.

Experimental section

The synthesis of pristine nitrogen-doped MWCNTs (MWCNT-CN_x) and ethanol synthesized MWCNTs (MWCNT-CO_x) were carried out by chemical vapor deposition (CVD). The CVD process was performed in an argon atmosphere carrying an aerosol containing 5 wt.% of ferrocene ($FeCp_2$) and 95 wt.% of benzylamine (C_7H_9N) for the MWCNT-CN_x [18], and with 1 wt.% ethanol and 5 wt.% of ferrocene in toluene (C_7H_8) for the MWCNT-CO_x [19]. These tubes were then acid treated in order to create structural defects (e.g. uncapped tubes, pyridine-like sites, and large vacancies) to facilitate the diffusion of liquid nitrogen into tube's core and within their external concentric cylinders, thus promoting the subsequent atomically smooth unzipping. The acid treatment was performed by adding 200 mg of MWCNTs in 30 ml of a solution of $H_2SO_4:HNO_3$ (3:1) and sonicated for 6 hours. After sonication, the resulting suspension was filtered and washed with deionized water and then dried. Subsequently, the acid treated MWCNTs (MWCNT-CO_x-A and MWCNT-CN_x-A) materials were kept on a receptacle with liquid nitrogen during 5 minutes. The abrupt unzipping occurs when adding boiling water to the recipient containing the acid treated nanotubes and liquid nitrogen. Since the temperature

changed from *ca.* -196°C to 45°C between 5 and 10 seconds, N₂ molecules inserted in previously created surface defects and in the hollow core of the concentric tubes undergoes a sudden thermal expansion giving rise to the unzipping of the nanotubes [20]. In addition, the dispersion was maintained under sonication at 80°C for 30 minutes. For the sake of comparison, the CO₂ adsorption characteristics of pure graphene (1-2 layers) from Avanzare Corp. (Spain) were also obtained. As it can be observed in Figure S1 (see Supporting Information), commercial graphene exhibits the typical structure consisting of corrugated graphene sheets.

Powder samples were characterized by scanning electron microscopy (SEM) using a FEI Helios 600 Nanolab equipment. The powders were also ultrasonically dispersed in isopropanol in order to carry out high-resolution transmission electron microscopy (HRTEM) studies using a Cs-corrector (2) equipped HR-TEM, JEM2100, JEOL, Japan.

X-ray photoelectron spectroscopy (XPS, K-ALPHA, Thermo Scientific) was used to analyze the samples surface. All spectra were collected using Al-K radiation (1486.6 eV), monochromatized by a thin crystal monochromator, yielding a focused X-ray spot with a diameter of 400 μm, at 3 mA x 12 kV. The alpha hemispherical analyzer was operated in the constant energy mode with survey scan pass energies of 200 eV to measure the wide scan and 50 eV in a narrow scan to selectively measure the particular elements. Charge compensation was achieved with the system flood gun that provides low energy electrons and low energy argon ions from a single source. The carbon sp²/sp³ ratio was estimated from the area of the XPS C1s signal at 284.2 eV, for C sp² and 285.1 eV, for C sp³, respectively. Additionally, the C/O ratio was estimated from the C1s and O1s signals.

Gas adsorption measurements (N₂ at -196°C and CO₂ at 0°C) at atmospheric pressure were performed in a home-made fully automated equipment designed and constructed by the

Advanced Materials Group (LMA), now commercialized as N₂-G-sorb-6 (Gas to Materials Technologies; www.g2mtech.com). Before any experiment, samples were degassed (10⁻⁸ MPa) at 523 K for 4h. BET surface area was calculated from the nitrogen adsorption data after application of the Brunauer-Emmett-Teller equation. Micropore volume (V_{N_2}) was estimated after application of the Dubinin-Radushkevich equation whereas the total pore volume (V_t) was taken as the amount adsorbed at a $p/p_0 \sim 0.9$.

Results and discussion

Scanning electron microscopy (SEM) images show that pristine MWCNT-CO_x and MWCNT-CN_x exhibit an average diameter of 64 nm and 74 nm, respectively (see Figure 1a and 1d). The unzipping process involves an intermediate step with acid treatment used to uncap the nanotube ends and intercalate sulfuric species within the outer layers of the MWCNT [20, 21]. Acid treated MWCNTs do not exhibit any apparent morphological changes besides the expected uncapping (see Figure 1b and 1e). Interestingly, a subsequent immersion of the acid treated MWCNTs in liquid nitrogen followed by a rapid rise in temperature results in the unzipping of MWCNTs so as to form graphene nanoribbons (see Figure 1c and 1f). In the case of MWCNT-CN_x, 46% of the nanostructures were longitudinally opened (nanoribbons termed here MWCNT-CN_x-NR), whereas in the case of the MWCNT-CO_x only 12% of the nanostructures were unzipped (termed here MWCNT-CO_x-NR). The observed behavior clearly shows the importance of nitrogen functionalities within MWCNTs for the successful thermally driven unzipping process. The nitrogen-doped nanoribbons exhibit curved belt/ribbon morphologies, as depicted in figures 1c and 1f. The edges of both nanoribbons MWCNT-CN_x-NR and MWCNT-CO_x-NR are similar under HRTEM, with sections of straight edges and others exhibiting some defects or

debris that resulted from the unzipping process (see Figure 2). As observed by electron microscopy, the nitrogen-doped and undoped MWCNTs, acid treated MWCNTs and nanoribbons possess similarities. However, the amounts of unzipped nanotubes depend upon N-doping, and this appears to be key for understanding the adsorption process.

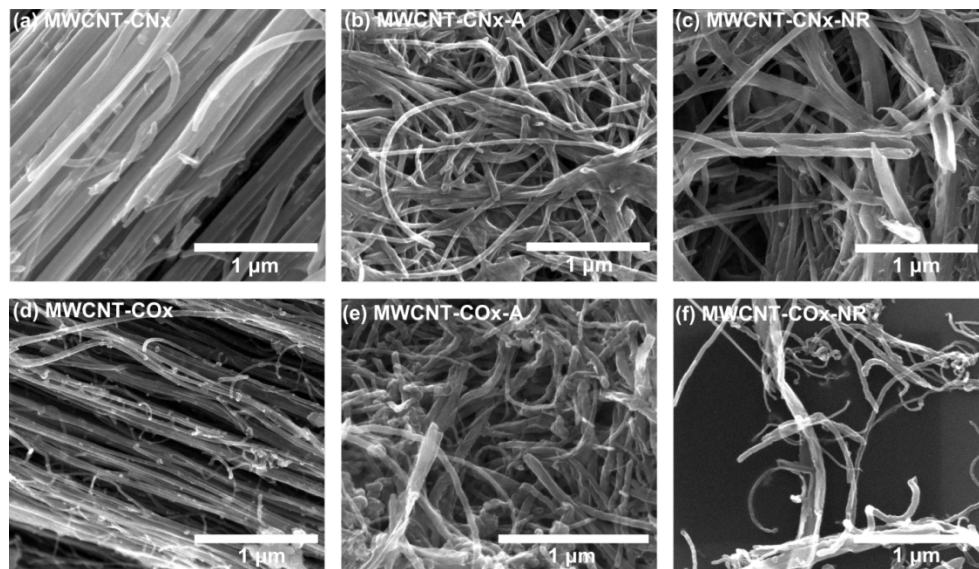


Figure 1: SEM images of the (a) pristine nitrogen doped carbon nanotubes (MWCNT-CN_x), (b) acid treated nitrogen-doped nanotubes (MWCNT-CN_x-A) and (c) nitrogen-doped graphene nanoribbons (MWCNT-CN_x-NR), (d) pristine pure carbon multiwalled nanotubes (MWCNT-CO_x), (e) acid treated MWCNT (MWCNT-CO_x-A) and (f) graphene nanoribbons (MWCNT-CO_x-NR).

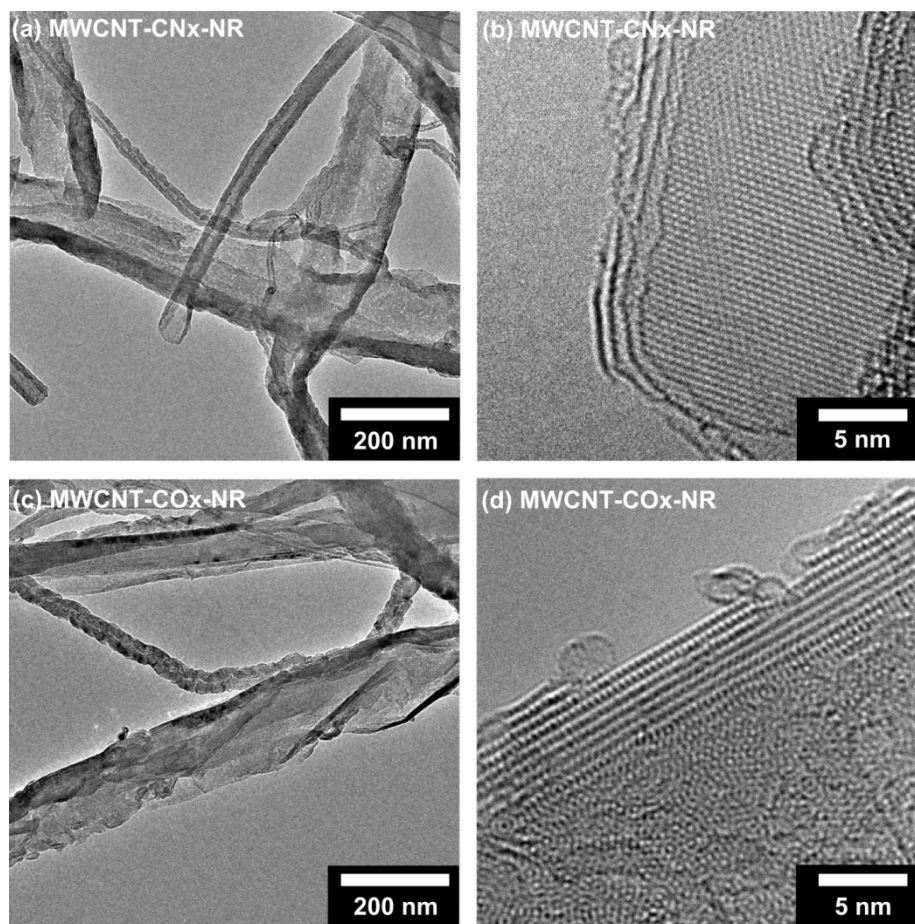


Figure 2: HRTEM images of the (a,b) nitrogen-doped and (c,d) non-doped graphene nanoribbons.

Textural properties of the synthesized samples were evaluated by nitrogen physisorption at cryogenic (-196°C) temperature. Table 1 contains a summary of the main textural properties, i.e., BET surface area, micropore volume and total pore volume for the different samples evaluated. As it can be observed, the original nanotubes exhibit a BET surface area *ca.* 90 m²/g and 30 m²/g for the MWCNT-CO_x and MWCNT-CN_x, respectively. These results are in close agreement with the larger tube diameter for the nitrogen-free nanotubes. In general, the acid treatment and the subsequent thermal expansion results in the slight increase in the BET surface area and micropore volume, although the changes in the N₂ physisorption isotherms are rather scarce (see Figure S2). Only sample MWCNT-CN_x-NR develops a type H4 hysteresis loop probably caused

by the nitrogen condensation in the mesocavities created after the nanotube unzipping, i.e. condensation in the curved regions within the nanoribbons. The scarce unzipping for the undoped nanotubes could explain the absence of any hysteresis loop in the MWCNT-CO_x-NR sample.

Additionally, Table 1 shows the sp^2/sp^3 ratio obtained after deconvolution of the XPS C1s signals. The sp^2/sp^3 ratio was calculated from the area of the deconvoluted peaks at 284.2 eV, for sp^2 , and 285.1 eV, for sp^3 [22, 23]. Pristine nanotube samples exhibit a large sp^2/sp^3 ratio caused by the absence of unsaturated carbon atoms or defects. As expected, the acid treatment gives rise to a drastic decrease in the sp^2/sp^3 ratio due to the opening of the nanotube ends and the formation of surface defective regions. Surprisingly, this ratio is not changing after the subsequent thermal shock (unzipping process), thus suggesting that the nanotube unzipping has no effect on the amount of surface defects (smooth unzipping), besides the formation of curved regions after the unzipping process. However, the formation of some steps and sharp edges after nanotube unzipping cannot be ruled out, as revealed by HRTEM. As described in the experimental section, pure graphene has been included as a standard material for graphitic nanostructures due to the combination of a large surface area together with few surface defects (high sp^2/sp^3 ratio), i.e., only unsaturated carbons are present in the plane boundary. The carbon to oxygen ratio (C/O) drastically decreases after the acid treatment and the subsequent “unzipping” process; the values being larger for the pure-carbon nanostructures. The observed decrease in the C/O ratio is mainly due to an edge oxidation process (edge functionalization with oxygen groups), first by removing the tube ends, and then by unzipping them into ribbons; the oxidation being facilitated in the nitrogen-doped samples. The overall nitrogen content from

the XPS surface analysis ranges from 2 atom %, on the pristine MWCNT-CN_x, to 1 atom %, on the acid-treated and unzipped samples.

The commercial graphene used exhibits the typical sheet-like morphology and consists of corrugated graphene sheets 1-2 layers thick (see Figure S1) with a BET surface area of approximately 290 m²/g. Although the BET surface area is not low, it is still less than the theoretical specific surface area of isolated graphene sheets, *ca.* 2620 m²/g. The nitrogen adsorption/desorption isotherm for graphene exhibits the traditional shape with a low adsorption capacity at low-medium relative pressures that corresponds to the low surface area together with a large capillary condensation at relative pressures close to 1 (see Figure S3). Furthermore, the desorption branch exhibits a large type H3 hysteresis loop due to the presence of specific interactions between the quadrupole moment of nitrogen and the graphene nanostructure, or more probably, due to the adsorption of N₂ molecules in the interlayer space between graphene sheets. The sp²/sp³ ratio for the graphene is as large as 8.2, thus reflecting the absence of important surface defects or sp³ hybridized carbons. The carbon to oxygen ratio for the graphene (7.32) is quite low when compared to the original MWCNT sample, *i.e.* the commercial graphene is rich in oxygen functionalities, although the C/O ratio is still quite high compared to that of graphene oxide and graphene oxide nanoribbons [24, 25].

Table 1. Compilation of textural properties calculated from the N₂ adsorption measurements at -196°C together with the CO₂ uptake at atmospheric pressure and 25°C. sp²/sp³ ratio and C/O ratio calculated from the XPS analysis is also included.

Sample	S _{BET} (m ² ·g ⁻¹)	V _{N2} (cm ³ ·g ⁻¹)	V _t (cm ³ ·g ⁻¹)	sp ² /sp ³	C/O	CO ₂ uptake (mg·g ⁻¹)
MWCNT-COx	90	0.03	0.12	7.01	36.6	0.88
MWCNT-COx-A	70	0.03	0.09	3.33	16.5	10.9
MWCNT-COx-NR	90	0.03	0.12	----	----	12.0
MWCNT-CNx	30	0.01	0.04	9.77	20.9	1.13
MWCNT-CNx-A	70	0.03	0.11	3.71	2.94	8.52
MWCNT-CNx-NR	70	0.02	0.10	3.87	1.85	18.8
Graphene	290	0.12	0.35	8.20	7.32	17.4

As described above, the presence of surface defects on graphitic nanostructures has a scarce effect on the adsorption of a traditional probe molecule such as nitrogen, with a quadrupole moment, at -196°C. However, a completely different scenario is observed in the case of CO₂ adsorption at 25°C. As observed in Figure 3, the adsorption capacity for CO₂ is highly affected by the carbon nanostructure. MWCNT-COx and MWCNT-CNx exhibit a low adsorption capacity, 0.88 mg/g and 1.13 mg/g, respectively (see Table 1). This observation is in close agreement with first principle calculations that predicted a weak adsorption for CO₂ on carbon nanotubes, either for surface, grooves or interstitial sites (~ 97-109 meV) [12]. Interestingly, the acid treatment produces a ten-fold increase in the amount of CO₂ adsorbed for both samples, this improvement being larger for the un-doped nanotubes (MWCNT-COx-A). Apparently, the uncapping of the nanotube ends and the formation of surface defective regions (low sp²/sp³ ratio) provide additional adsorption sites with enhanced adsorbate-adsorbent interactions for CO₂.

Theoretical calculations predict an improvement in the CO₂ adsorption energy for graphitic surfaces in the presence of oxygen functionalities [15]. According to XPS analysis, the amount of oxygen surface groups increases after the acid treatment with H₂SO₄/HNO₃ for both samples (see Table 1), although this increase is much larger for the nitrogen-doped sample. Consequently, the larger improvement in the CO₂ adsorption capacity in the pure carbon nanotubes cannot exclusively be attributed to the incorporation of oxygen functionalities after acid treatment, but rather to the formation of surface defects (decrease in the sp²/sp³ ratio) after uncapping the nanotube ends. This statement will be in correlation with experimental analysis on activated carbons which predict a scarce effect of the oxygen surface groups in the adsorption of CO₂, despite theoretical predictions [26]. A subsequent unzipping of the acid treated nanotubes produces a different effect depending on the sample composition. Although there is a slight improvement in the adsorption capacity for MWCNT-CO_x (up to 12.02 mg/g), this improvement is extremely large for MWCNT-CN_x (up to 18.83 mg/g). The high adsorption capacity of the nitrogen-doped graphene nanoribbons could be associated to: i) the presence of a larger proportion of surface defects (although not detected by XPS), ii) the presence of inner tubular curved regions accessible after the thermal expansion (unzipping), iii) the higher oxygen content after the unzipping (C/O ratio 1.85), and (iv) the presence of step like defects and terraces characteristic of CN_x nanotubes that might provide CO₂ adsorption sites, in a similar fashion to other graphitic nanostructures [27]. In this sense, the absence of a large improvement in the CO₂ adsorption capacity for MWCNT-CO_x could be attributed to the inefficient unzipping (only 12% of the nanotubes are unzipped). Interestingly, CO₂ adsorption isotherms for the different nitrogen-doped carbon nanostructures exhibit the well-known hysteresis at low pressures [28]. The presence of the low-pressure hysteresis loop in our nitrogen-doped samples must be

attributed, not to the lack of equilibrium but rather to the irreversible adsorption of CO₂ on the surface-nitrogen functionalities. Nitrogen surface groups are highly electronegative and thus can serve as basic adsorption sites on the basal planes exhibiting an improved adsorbent-adsorbate interaction.

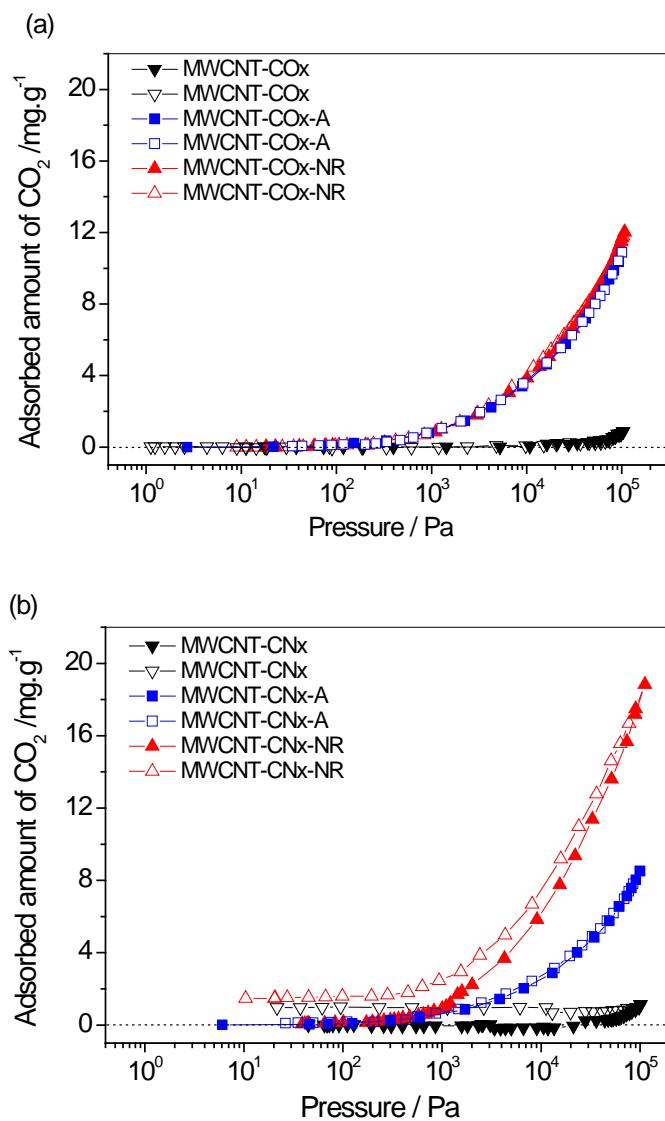


Figure 3. CO₂ adsorption isotherms for (a) pure carbon and (b) nitrogen doped samples up to atmospheric pressure and 25°C.

Finally, the adsorption behavior of the nitrogen-doped nanoribbons (MWCNT-CN_x-NR) was compared with the one of a more ordered graphitic nanostructure such as graphene that contains large basal planes with a low proportion of surface defects (sp^2/sp^3 ratio of 8.2), as well as a relatively important oxygen content (C/O ratio 7.32), although smaller than that of the nitrogen-doped nanoribbons (C/O ratio 1.85). As it can be observed in Figure 4, the CO₂ adsorption capacity in the low relative pressure range is enhanced for the nitrogen-doped nanoribbons when compared to pure graphene. The upward deviation at 10³ Pa in the nanoribbons must be attributed both to the presence of curved regions, with a high adsorption potential, and the presence of nitrogen functionalities. Interestingly, and in spite of the lower BET surface area, the amount of CO₂ adsorbed on the nanoribbons is always higher than that of pure graphene, thus suggesting that the adsorption capacity on graphitic nanostructures is not defined by the total BET surface area, as suggested for porous carbons, neither by the presence of oxygen functionalities, but rather by the presence of surface defects (rough edges), curved regions and, to a lower extent, to surface nitrogen functionalities. Consequently, surface defects, curved regions and surface nitrogen functionalities should be considered as the critical adsorption sites for CO₂ capture on graphitic nanostructures. Furthermore, both samples exhibit a delay between the adsorption and the desorption branch. For nitrogen-doped nanoribbons this delay must be attributed to the presence of strong surface adsorption sites with enhanced adsorbate-adsorbent interactions, as described above, whereas for graphene must be attributed to the intercalation of CO₂ in the interlayer space during the adsorption process.

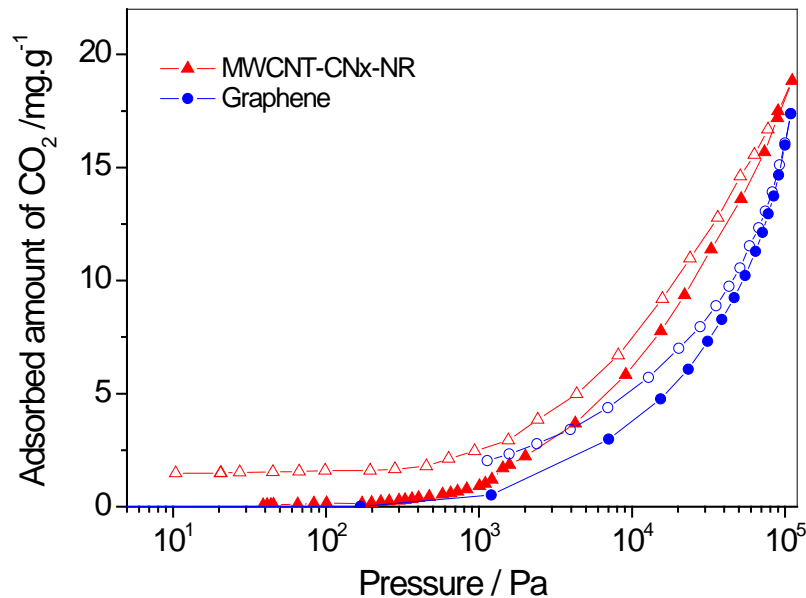


Figure 4. CO₂ adsorption capacity for nitrogen-doped graphene nanoribbons (MWCNT-CN_x-NR) and pure graphene at 25°C.

Conclusions

CO₂ capture has been evaluated in different types of graphitic nanostructures (MWCNTs, acid treated MWCNTs, unzipped MWCNTs (graphene nanoribbons) and pure graphene) in order to elucidate the effect of the different surface defects (sp^2/sp^3 ratio, curved regions, step like terraces and so on), and surface functionalities in the adsorption process. Experimental results demonstrate that the adsorption capacity is mainly defined by the presence of surface defects (rough edges) and curved regions; the effect of the oxygen surface groups being rather small. The maximum adsorption capacity was observed for the nitrogen-doped graphene nanoribbons due to the higher efficiency of the unzipping process and the larger proportion of surface/edge defects and curved regions.

Acknowledgement

Authors acknowledge financial support from the MICINN (project PLE2009-0052) and Generalitat Valenciana (PROMETEO/2009-002). SMVD, FTL, HM, TH, RCS, MT, and ME acknowledge support from the Research Center for Exotic Nanocarbons, Japan regional Innovation Strategy Program by the Excellence, JST. AMG acknowledges support from NEDO for postdoctoral position.

References

- [1] J.D. Figueroa, T. Fout, S. Plasynski, H. McIlvried, R.D. Srivastava, *Int. J. Greenhouse Gas Control* 2 (2008) 9-20.
- [2] D.M. D'Alessandro, B. Smit, J.R. Long, *Angew. Chem. Int. Ed.* 49 (2010) 6058-6082.
- [3] A. Wahby, J.M. Ramos-Fernández, M. Martínez-Escandell, A. Sepúlveda-Escribano, J. Silvestre-Albero, F. Rodríguez-Reinoso, *ChemSusChem* 3 (2010) 974-981.
- [4] V. Presser, J. McDonough, S-H. Yeon, Y. Gogotsi, *Energ. Environm. Sci.* 4 (2011) 3059-3066.
- [5] J. Silvestre-Albero, A. Wahby, A. Sepúlveda-Escribano, M. Martínez-Escandell, K. Kaneko, F. Rodríguez-Reinoso, *Chem. Commun.* 47 (2011) 6840-6842.
- [6] M. Sevilla, A.B. Fuertes, *Energ. Environm. Sci.* 4 (2011) 1765-1771.
- [7] D.P. Vargas, L. Giraldo, J. Silvestre-Albero, J.C. Moreno-Piraján, *Adsorption* 17 (2011) 497-504.
- [8] M. Sevilla, P. Valle-Vigón, A.B. Fuertes, *Adv. Funct. Mater.* 21 (2011) 2781-2787.
- [9] X. Zhu, P.C. Hillesheim, S.M. Mahurin, C. Wang, C. Tian, S. Brown, H. Luo, G.M. Veith, K.S. Han, E.W. Hagaman, H. Liu, S. Dai, *ChemSusChem* 5 (2012) 1912-1917.
- [10] J.A. Thote, K.S. Iyer, R. Chatti, N.K. Labhsetwar, R.B. Biniwale, S.S. Rayalu, *Carbon* 48 (2010) 396-402.
- [11] C. Pevida, M.G. Plaza, B. Arias, J. Feroso, F. Rubiera, J.J. Pis, *Appl. Surf. Sci.* 254 (2008) 7165-7172.
- [12] J. Zhao, A. Buldum, J. Han, J.P. Lu, *Nanotechnology* 13 (2002) 195-200.
- [13] A. Ghosh, K.S. Subrahmanyam, K.S. Krishna, S. Datta, A. Govindaraj, S.K. Pati, C.N.R. Rao, *J. Phys. Chem. C* 112 (2008) 15704-15707.
- [14] Y. Liu, J. Wilcox, *Environ. Sci. Technol.* 46 (2012) 1940-1947.
- [15] P. Cabrera-Sanfeliu, *J. Phys. Chem. A* 113 (2009) 493-498.
- [16] W.L. Yim, O. Byl, J.T. Yates, J.K. Johnson, *J. Chem. Phys.* 120 (2004) 5377-5387.
- [17] J. Jiang, S.I. Sandler, *J. Am. Chem. Soc.* 127 (2005) 11989-11997.
- [18] M. Terrones, R. Kamalakaran, T. Seeger, M. Rühle, *Chem. Commun.* (2000) 2335-2336.
- [19] A. Botello-Méndez, J. Campos-Delgado, A. Morelos-Gómez, J.M. Romo-Herrera, A.G. Rodríguez, H. Navarro, M.A. Vidal, H. Terrones, M. Terrones, *Chem. Phys. Lett.* 453 (2008) 55-61.
- [20] A. Morelos-Gómez, S. Magdalena Vega-Díaz, V. J. González, F. Tristán-López, R. Cruz-Silva, K. Fujisawa, H. Muramatsu, T. Hayashi, X. Mi, Y. Shi, H. Sakamoto, F. Khoerunnisa, K.

- Kaneko, B. G. Sumpter, Y. A. Kim, V. Meunier, M. Endo, E. Muñoz-Sandoval, M. Terrones, *ACS Nano* 6 (2012) 2261–2272.
- [21] A. Morelos-Gómez, S. Magdalena Vega-Díaz, V. J. González, F. Tristán-López, R. Cruz-Silva, K. Fujisawa, H. Muramatsu, T. Hayashi, X. Mi, Y. Shi, H. Sakamoto, F. Khoerunnisa, K. Kaneko, B. G. Sumpter, Y. A. Kim, V. Meunier, M. Endo, E. Muñoz-Sandoval, M. Terrones, *World Academy of Sci., Eng. & Techn.* 61 (2012) 1167-1171.
- [22] H. Ago, T. Kugler, F. Cacialli, W.R. Salaneck, M.S.P. Shaffer, A.H. Windle, R.H. Friend, *J. Phys. Chem. B* 103 (1999) 8116-8121.
- [23] W.-J. Chou, C.-C. Wang, C.-Y. Chen, *J. Inorg. Organomet. Polym.* 19 (2009) 234-242.
- [24] D. C. Marcano, D.V. Kosynkin, J. M. Berlin, A. Sinitskii, Z. Sun, A. Slesarev, L.B. Alemany, W. Lei, J.M. Tour, *ACS Nano* 4 (2010) 4806-4814.
- [25] A.L. Higginbotham, D.V. Kosynkin, A. Sinitskii, Z. Sun, J.M. Tour, *ACS Nano* 4 (2010) 2059-2069.
- [26] G. Yin, Z. Liu, Q. Liu, W. Wu, *Chem. Eng. J.* 230 (2013) 133-140.
- [27] M. Asai, T. Ohba, T. Iwanaga, H. Kanoh, M. Endo, J. Campos-Delgado, M. Terrones, K. Nakai, K. Kaneko, *J. Am. Chem. Soc.* 133 (2011) 14880-14883.
- [28] A. M. Silvestre-Albero, J.M. Juárez-Galán, J. Silvestre-Albero, F. Rodríguez-Reinoso, *J. Phys. Chem. C* 116 (2012) 16652-16655.